inter.noise
27-30 AUGUST HONG KONG 2017

Synchrophase vibration control for isolated rotating machines

Di HUANG[1]; Neil FERGUSON[2]; Tiejun YANG[1]; Xinhui LI[1]; Zhigang LIU[1]; Minggang Zhu[1]

[1]Harbin Engineering University, People's Republic of China

[2] University of Southampton, UK

ABSTRACT

In this paper, a machinery installation is described, in which several rotational machines are attached to a machinery beam-like raft by discrete resilient isolations. To reduce the vibration of the host raft introduced by the machines installed to the raft, a vibration control method of altering only the phases between the machines, known as synchrophasing, is investigated both theoretically and experimentally. A method, known as Propeller Signature Theory (PST) is used to determine the generalized transfer mobility matrix, by which the full search approach is then used to find the optimum phase angle. It is shown that the synchrophasing can achieve a significant vibration reduction when there are only two machines. Meanwhile, as each machine is supported by discrete rubber isolation mounts, the effect of the stiffness of the isolations is also discussed from the results of further simulation.

Keywords: Synchrophasing, vibration control, Effect of discrete isolations

1. INTRODUCTION

As a widely-employed and traditional vibration control method, passive isolators can achieve quite effective reduction of the vibration transmitted from such sources as rotating machines attached to a host structure especially in the high frequency range. In the lower frequency bands, however, the passive isolators will come across a trade-off between the efficiency of the isolation performance and the stability of the whole system or the weight cost. Therefore, alternative approaches, e.g. active control, is typically introduced by applying some secondary sources in series or parallel with passive resilient mounts to generate forced vibration responses aiming to cancel the primary vibration transmission [1,2]. However, the active control method using any type of different actuators will need a back-up system including power amplifiers, digital controllers and so on. This could be very expensive and power-consuming.

Synchrophasing is another alternative control method considered in this paper, which has been well verified and established in the area of propeller noise control in aircraft cabins [3]. The basic idea of synchrophasing is quite simple, coming from the idea of reducing the vibrations originating from two engines of a steam ship by making the two engines run at the same speed, but in anti-phase [4]. Apart from the patent obtained by Kalin, for a method of controlling vibration introduced by the main propulsion diesel engines of a ship with multiple propellers by maintaining a constant phase angle between the crank shafts in 1940, several patents and literature on noise control in aircraft cabins [5, 6] and duct [7, 8] have been published as well as two patents for reducing sound and/or vibration from multiple rotating machines [9, 10], by adjusting the phase angle between the propellers or machines. Further research in this area has been extended to active synchrophasing. Microphones and accelerometers were introduced and positioned throughout an aircraft as the error signal in an adaptive algorithm, that were used to determine the optimum phase angle for minimizing the cabin noise and vibration over a wider range of flight conditions [11, 12]. In this process, to reduce the time needed to obtain the optimum phase angle, the Propeller Signature Theory

1. huangdi@hrbeu.edu.cn
2. nsf@isvr.soton.ac.uk

(PST) described in [13] was employed.

A few studies on controlling vibration transmission from a machinery raft to a host structure by adjusting the phase angles between the machines has also been reported. Recent research on synchrophasing by Dench and Brennan [14] demonstrated the principle of this method on a one-dimensional structure. They considered theoretically the behaviour of a machinery raft, together with an experimental study, to illustrate the application of synchrophasing to multiple machines for a marine application. The PST and an exhaustive search of all possible angles were used to determine the optimum phase angles for different scenarios. Yang subsequently extended this control method to a large scale floating raft system, where multiple machines were attached theoretically and then validated is experimentally [15].

This paper is an extension of the work by Dench et al [14]. The application of synchrophasing to vibration control on the same one-dimensional structure is investigated, while each source is attached to the raft though a support plate and four passive isolators. In this case, both forces and moments introduced by the sources are taken into account i.e. the excitation sources themselves are allowed to have a primary stage of isolation. The effect of the primary isolation stage is discussed using the numerical model.

2. PROBLEM FORMULATION

2.1 Lumped parameter model

The idealised lumped parameter model used to investigate and determine the performance of synchrophasing and the effect of isolation of the sources is shown in Figure 1. Two potentially synchronous machines are resiliently attached to a long raft, which is supported by two identical elastic springs at its ends respectively. The machines and the raft can all be considered as rigid bodies, therefore only the displacement and the rotation of each inertia needs to be taken into account i.e. the model is then a 6-freedom-degree system.

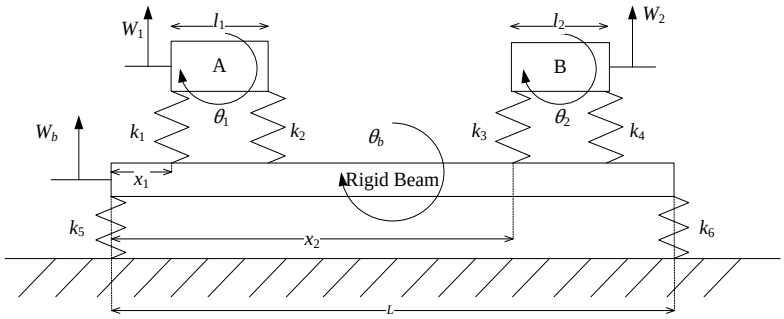

Figure 1. The model and parameters of the simulated system.

Based on the D'Alembert's principle, the equations of motion for each inertia can be written in a matrix form as follows

$$\mathbf{M}\ddot{\mathbf{w}} + \mathbf{K}\mathbf{w} = \mathbf{f} \tag{1}$$

where **M**, **K** are the two respective mass and stiffness matrices and **w**, **f** are the respective degrees of freedom and source forces acting at the respective degree of freedom.

For the system shown in Figure 1, the 6×6 mass matrix is $\mathbf{M} = \begin{bmatrix} m_1 & 0 & 0 & 0 & 0 & 0 \\ 0 & J_1 & 0 & 0 & 0 & 0 \\ 0 & 0 & m_2 & 0 & 0 & 0 \\ 0 & 0 & 0 & J_2 & 0 & 0 \\ 0 & 0 & 0 & 0 & m_b & 0 \\ 0 & 0 & 0 & 0 & 0 & J_b \end{bmatrix}$, the

corresponding stiffness matrix

$$\mathbf{K}=\begin{bmatrix} k_1+k_2 & -\frac{k_1l_1}{2}+\frac{k_2l_1}{2} & 0 & 0 & -k_1-k_2 & K_1 \\ -\frac{k_1l_1}{2}+\frac{k_2l_1}{2} & \frac{k_1l_1^2}{4}+\frac{k_2l_1^2}{4} & 0 & 0 & \frac{k_1l_1}{2}-\frac{k_2l_1}{2} & K_2 \\ 0 & 0 & k_3+k_4 & -\frac{k_3l_2}{2}+\frac{k_4l_2}{2} & -k_3-k_4 & K_3 \\ 0 & 0 & -\frac{k_3l_2}{2}+\frac{k_4l_2}{2} & \frac{k_3l_2^2}{4}+\frac{k_4l_2^2}{4} & \frac{k_3l_2}{2}-\frac{k_4l_2}{2} & K_4 \\ -k_1-k_2 & \frac{k_1l_1}{2}-\frac{k_2l_1}{2} & -k_3-k_4 & \frac{k_3l_2}{2}-\frac{k_4l_2}{2} & k_1+k_2+k_3+k_4+k_5+k_6 & K_5 \\ K_1 & K_2 & K_3 & K_4 & K_5 & K_6 \end{bmatrix}$$

where $K_1=-k_1\left(\frac{L}{2}-x_1\right)+k_2\left(l_1+x_1-\frac{L}{2}\right)$, $K_2=\frac{k_1l_1}{2}\left(\frac{L}{2}-x_1\right)+\frac{k_2l_1}{2}\left(l_1+x_1-\frac{L}{2}\right)$,

$K_3=-k_3\left(\frac{L}{2}-x_2\right)+k_4\left(l_2+x_2-\frac{L}{2}\right)$, $K_4=\frac{k_3l_2}{2}\left(\frac{L}{2}-x_2\right)+\frac{k_4l_2}{2}\left(l_2+x_2-\frac{L}{2}\right)$,

$K_5=k_1\left(\frac{L}{2}-x_1\right)-k_2\left(l_1+x_1-\frac{L}{2}\right)+k_3\left(\frac{L}{2}-x_2\right)-k_4\left(l_2+x_2-\frac{L}{2}\right)+k_5\frac{L}{2}-k_6\frac{L}{2}$

$K_6=k_1\left(\frac{L}{2}-x_1\right)^2+k_2\left(l_1+x_1-\frac{L}{2}\right)^2+k_3\left(\frac{L}{2}-x_2\right)^2+k_4\left(l_2+x_2-\frac{L}{2}\right)^2+k_5\frac{L^2}{4}+k_6\frac{L^2}{4}$

and the corresponding degrees of freedom expressed as a displacement vector is

$$\mathbf{w}=\begin{bmatrix} w_{M_1} & \theta_{M_1} & w_{M_2} & \theta_{M_2} & w_b & \theta_b \end{bmatrix}^{\mathrm{T}} \tag{2}$$

The degrees of freedom chosen for modelling this scenario are respectively the three translations of the centres of mass and three rotations about the centres of masses of the two sources and one receiver mass, i.e. w_{M_1}, w_{M_2}, w_b and θ_{M_1}, θ_{M_2}, θ_b. The subscripts M_1, M_2, b relate to the displacements of machine A, machine B, raft and the corresponding rotation of each inertia mass respectively. Meanwhile, k_1, k_2, k_3, k_4, k_5 and k_6 are the stiffnesses of the springs connected between the machine masses and the host structure and between the raft and the fixed ground. m_1, m_2 and m_b are the masses of two machines as well as the raft; J_1, J_2 and J_3 the corresponding rotational inertia of the three masses about their corresponding mass centres. L is the length of the raft on which the positions of the left hand end of the two machines are represented by x_1 and x_2 respectively, which can be seen in Figure 1. l_1 and l_2 are the lengths of the two machines.

The excitation of each machine is assumed to be introduced by the rotational motion of an out of balance motor, which both produces an equivalent vertical force and a moment that are assumed harmonic and at the same circular frequency ω. In general, there is a phase difference φ between the excitations of the two machines. That then gives the excitation force matrix in the terms of the magnitudes as well as the phases which will simplify the derivation

$$\mathbf{f}=\begin{bmatrix} F_1 & F_1\sigma_1 & F_2e^{-j\varphi} & F_2\sigma_2e^{-j\varphi} & 0 & 0 \end{bmatrix}^{\mathrm{T}}\times e^{j\omega t}=\mathbf{F_n}e^{j\omega t} \tag{3}$$

where F_1, F_2 are the amplitudes of the forces generated by the machines and σ_1, σ_2 are the distances between the out of balance forces produced in the machines and the centres of the machines, which then provides the moment excitation. φ is the phase between the two out of balance sources, noting the reference source being the source on mass A(subscript 1). No direct excitation is assumed on the raft, only internal forces due to the isolation springs acting between the raft and isolated machines.

Also, the displacement vector can be rewritten in the same way, which gives

$$\mathbf{w} = \begin{bmatrix} W_{M_1} & \Theta_{M_1} & W_{M_2} & \Theta_{M_2} & W_b & \Theta_b \end{bmatrix}^{\mathrm{T}} \times e^{j\omega t} = \mathbf{W} e^{j\omega t} \tag{4}$$

From equation (1), the steady solution of the forced vibration of the 6-freedom-degree undamped system can be derived, which can be given in matrix form as

$$\mathbf{W} = [\mathbf{K} - \omega^2 \mathbf{M}]^{-1} \mathbf{F}_n \tag{5}$$

In addition, if the system is vibrating freely, the external forces generated by the machines are zero. Then the characteristic matrix of the system is given by

$$\mathbf{S} = [\mathbf{K} - \omega^2 \mathbf{M}] \tag{6}$$

Consider that the system contains structural damping, equation (5) becomes

$$\mathbf{W} = [(1 + j\eta)\mathbf{K} - \omega^2 \mathbf{M}]^{-1} \mathbf{F}_n \tag{7}$$

Where, for simplicity, the same proportional damping is assumed for all stiffness components in the model, i.e. η indicates the damping loss factor, assumed to be the same throughout. In this way, the numerical solutions for W_{M_1}, W_{M_2}, W_b and Θ_{M_1}, Θ_{M_2}, Θ_b are all in general complex.

Separating the 6-order matrix $\boldsymbol{\alpha} = [(1 + j\eta)\mathbf{K} - \omega^2 \mathbf{M}]^{-1}$ in equation (7), known as the receptance matrix, into nine 2-order block matrices $\boldsymbol{\alpha}_{ij}$; therefore the motion vector of the raft can be given by

$$\mathbf{w}_B = \mathbf{W}_B e^{j\omega t} \tag{8}$$

in which $\mathbf{W}_B = \begin{bmatrix} w_b & \theta_b \end{bmatrix}^{\mathrm{T}}$ denotes the amplitude of the motion of the raft and can be written in terms of a sub-matrices of $\boldsymbol{\alpha}$ and the applied force vector $\mathbf{F}_n$, i.e.

$$\mathbf{W}_B = \begin{bmatrix} \boldsymbol{\alpha}_{31} & \boldsymbol{\alpha}_{32} & \boldsymbol{\alpha}_{33} \end{bmatrix} \mathbf{F}_n \tag{9}$$

where the subscript 31, 32 and 33 denote the positions of the sub-matrix in the original full matrix for $\boldsymbol{\alpha}$.

2.2 Cost function definition and choice for vibration control

One requirement for vibration control might be the reduction of the transmitted forces though the isolations of the raft. This would suggest reducing the motion at the attachment points of the lower isolation to the raft. A consequence might be some reduction of the raft response specially averaged but this is not guaranteed

To capture the motion of the raft for subsequent comparison of the response under different synchrophase situations, a suitable cost function can be given as

$$J = \dot{\mathbf{w}}_e^{\mathrm{H}} \dot{\mathbf{w}}_e \tag{10}$$

for which $\dot{\mathbf{w}}_e$ is the vector of the two end velocities of the raft and the superscript H denotes the Hermitian transpose. This produces a cost function J which is simply the sum of the squares of the two modulus of the velocities. The velocity vector $\dot{\mathbf{w}}_e$ can be expressed in terms of the raft degrees of freedom as

$$\dot{\mathbf{w}}_e = \mathbf{L}\dot{\mathbf{w}}_B = \begin{bmatrix} 1 & \frac{L}{2} \\ 1 & -\frac{L}{2} \end{bmatrix} \begin{bmatrix} \dot{w}_b \\ \dot{\theta}_b \end{bmatrix} \tag{11}$$

for which the square matrix **L** is the transfer matrix between the ends and the centre of mass degrees of freedom.

Combining Equations (8), (9), (10) and (11) gives the cost function in terms of the transfer matrix and the system receptances.

$$J = \dot{\mathbf{w}}_B^{\mathrm{H}} \mathbf{L}^{\mathrm{H}} \mathbf{L} \dot{\mathbf{w}}_B = -\omega^2 \mathbf{W}_B^{\mathrm{H}} \mathbf{L}^{\mathrm{H}} \mathbf{L} \mathbf{W}_B = -\omega^2 \mathbf{F}_n^{\mathrm{H}} \begin{bmatrix} \boldsymbol{\alpha}_{31} & \boldsymbol{\alpha}_{32} & \boldsymbol{\alpha}_{33} \end{bmatrix}^{\mathrm{H}} \mathbf{L}^{\mathrm{H}} \mathbf{L} \begin{bmatrix} \boldsymbol{\alpha}_{31} & \boldsymbol{\alpha}_{32} & \boldsymbol{\alpha}_{33} \end{bmatrix} \mathbf{F}_n \tag{12}$$

Equation (12) can be rewritten as

$$J = \boldsymbol{\Phi}^{\mathrm{H}} \boldsymbol{\Gamma}^{\mathrm{H}} \boldsymbol{\Gamma} \boldsymbol{\Phi} \tag{13}$$

where $\boldsymbol{\Gamma} = j\omega \boldsymbol{\alpha} \mathbf{A}$ and $\mathbf{A} = \begin{bmatrix} F_1 & 0 & 0 & 0 & 0 & 0 \\ 0 & F_1\sigma_1 & 0 & 0 & 0 & 0 \\ 0 & 0 & F_2 & 0 & 0 & 0 \\ 0 & 0 & 0 & F_2\sigma_2 & 0 & 0 \\ 0 & 0 & 0 & 0 & 0 & 0 \\ 0 & 0 & 0 & 0 & 0 & 0 \end{bmatrix}$ is the amplitude of the forces present, while the phase of the forces is given by the vector $\boldsymbol{\Phi} = \begin{bmatrix} 1 & 1 & e^{-j\varphi} & e^{-j\varphi} & 0 & 0 \end{bmatrix}^{\mathrm{T}}$. In this case, as the 'transfer function' matrix $\boldsymbol{\Gamma}$ is independent of the phase between the forces introduced by the machines and it is just frequency related, it is relatively easy to determine the optimum phase angle φ of the secondary source with respect to the primary source for certain working conditions or frequency.

2.3 Synchrophasing and achieving control

As mentioned above, synchrophasing is an approach whereby altering the phase angles between the synchronous machines, such as electric motors etc., the vibration of the host structure onto which the machines are resiliently attached can be reduced.

A cost function to denote the vibration of the host raft has been described in the former section and it can be rewritten as follows in a more general way by which one can acquire the principal method to get the optimal value of the cost function using synchrophasing.

$$\hat{J} = \hat{\boldsymbol{\Phi}}^{\mathrm{H}} \begin{bmatrix} \boldsymbol{\gamma}_1^{\mathrm{H}} \boldsymbol{\gamma}_1 & \boldsymbol{\gamma}_1^{\mathrm{H}} \boldsymbol{\gamma}_2 & \cdots & \boldsymbol{\gamma}_1^{\mathrm{H}} \boldsymbol{\gamma}_{2(n+1)} \\ \boldsymbol{\gamma}_2^{\mathrm{H}} \boldsymbol{\gamma}_1 & \boldsymbol{\gamma}_2^{\mathrm{H}} \boldsymbol{\gamma}_2 & \cdots & \boldsymbol{\gamma}_2^{\mathrm{H}} \boldsymbol{\gamma}_{2(n+1)} \\ \vdots & \vdots & \ddots & \vdots \\ \boldsymbol{\gamma}_{2n}^{\mathrm{H}} \boldsymbol{\gamma}_1 & \boldsymbol{\gamma}_{2n}^{\mathrm{H}} \boldsymbol{\gamma}_2 & \cdots & \boldsymbol{\gamma}_{2(n+1)}^{\mathrm{H}} \boldsymbol{\gamma}_{2(n+1)} \end{bmatrix} \hat{\boldsymbol{\Phi}} \tag{14}$$

where $\hat{\boldsymbol{\Phi}}$ is a 2(n+1)-length vector that shows the phase angles of the n machines that will introduce both force and moment in the same time and $\boldsymbol{\gamma}_i$ is a Q-length vector that denotes the generalized transfer mobility containing the force and the moment information as well from the i^{th} machine to Q identified positions at which the velocities are used to determine the corresponding cost function.

Furthermore, Eq. (14) can be written as the sum of three parts, so that

$$\hat{J} = J_A + J_B + J_C \tag{15}$$

for which

$$J_A = \sum_{i=1}^{n} \left\| \boldsymbol{\gamma}_i \right\|^2 \tag{16a}$$

$$J_B = 2 \sum_{i=1}^{2(n+1)} \mathrm{Re}\left\{ \boldsymbol{\gamma}_1{}^{\mathrm{H}} \boldsymbol{\gamma}_i e^{j(\varphi_i - \varphi_1)} \right\} \tag{16b}$$

$$J_C = 2 \sum_{i=2}^{2(n+1)} \sum_{j=3}^{2(n+1)} \mathrm{Re}\left\{ \boldsymbol{\gamma}_i{}^{\mathrm{H}} \boldsymbol{\gamma}_j e^{j(\varphi_j - \varphi_i)} \right\} \Bigg|_{i \neq j} \tag{16c}$$

Note that for the three parts of the cost function $\hat{J}$, Equation (16a) shows that the first part J_A is the sum of the terms on the leading diagonal of the inner matrix in Equation (15), i.e. the general transfer mobility contains no phase information; therefore, changing the phase angle would not change the value of J_A. Equation (16b) gives the direct relationship between the phase angle between the control machines and the reference machine. The third part of the cost function J_C includes the interaction between the control machines where there are three or more machines.

Normally, the mobility vectors can be evaluated by measuring the accelerations at the identical positions and gathering the input signal to each machine when the machine is driven by an input signal which is band limited random noise.

3. NUMERICAL SIMULATIONS FOR ISOLATED MACHINES

Of interest in this section is to determine the influence of the phase angle between the two machines, the effect of the isolation and also whether the harmonic out of balance excitations are acting at frequencies above or below the isolation frequency for the machines.

3.1 Performance of synchrophasing

For numerical simulations and results, complemented by later experimental validation, the following parameters were assumed: m_1 =1.85kg, m_2 = 1.82kg, m_b = 2.3kg, L = 1.2m, l_1 = 0.4m, l_2 = 0.3m, x_1 = 0.1m, x_2 = 0.85m, k_1 = k_2 = k_3 = k_4 = 2.34×10^4Nm^{-1}, k_5 = k_6 = 1.94×10^4Nm^{-1}. The rotational inertia were consequently calculated to be $J_1 = 0.025 kgm^2$, $J_2 = 0.01 kgm^2$, $J_3 = 0.28 kgm^2$. In this particular case, the two machines are on opposite sides of the centre of mass of the raft.

Substituting the numbers into the equation (6), the six natural frequencies as well as the corresponding modal shape are given in Table 1 below.

Table 1. Natural frequencies and mode shapes of the system

Natural frequency/Hz	11.84	17.42	40.14	44.07	44.30	57.37
Mode shape as a vector of the degrees of freedom $\left[W_{M_1} \quad \Theta_{M_1} \quad W_{M_2} \quad \Theta_{M_2} \quad W_b \quad \Theta_b\right]^{\mathrm{T}}$	0.42	-0.48	0.22	-0.06	0.26	0.10
	0.05	0.85	4.43	3.85	-0.53	-2.26
	0.46	0.47	-0.11	-0.05	0.26	-0.18
	0.05	0.85	4.09	-6.62	-2.56	-2.35
	0.35	-0.04	-0.12	0.11	-0.53	0.07
	-0.05	-0.72	-0.72	0.04	-0.01	-1.61

From Table 1, it can be clearly seen that the fundamental mode of the system is mainly the vertical displacement of the three masses and the sixth mode is primarily the rotation of the machines and raft. The fifth mode is the rotation of the secondary machine, whilst the second mode cannot be so specifically described as they comprise both displacements of and rotations about the centres of mass of the three bodies. For the third and fourth natural frequencies, the rotations of two machines both dominate, while since the fourth natural frequency is quite close to the fifth one, the rotational motion of the secondary machine is more dominant.

For the simulations, the force and moment introduced by machine A are taken into account as the reference excitation, whilst the forces that are generated by machine B are the control sources. In addition, assuming the excitation source is due to unbalance, the magnitudes of the forces are in proportion to the square of the rotational speeds of the machines and the moment amplitudes are the products of the forces and the eccentricities of the sources about the machine mass centres. Therefore, in the present numerical simulations one can assume that the magnitudes of the forces F_1 and F_2 are proportional to $3\omega^2$ and $2.5\omega^2$ respectively with the corresponding eccentricities are 0.2m and 0.15m respectively. The loss factor was assumed constant and equal 0.05.

By altering the phase angle between the two machines, a full search through the phase angle from 0 ºto 360 º in step size of 7.2 º was used to determine the optimum phase angle between the two machines to minimize or maximize the value of the cost function in the frequency band of 1Hz to 200Hz which covers the first six resonances. For this situation, the reference source was at $x_1 / L = 1/12$ and control source was at $x_2 / L = 17/24$.

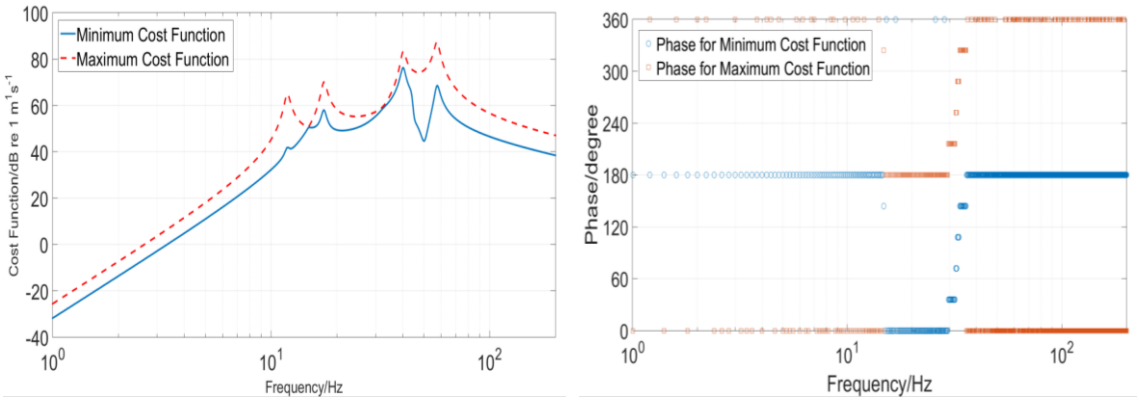

(a) (b)

Figure 2. Plots of the minimum (blue solid line) and maximum (red dash line) cost function obtained searching the sum of the squared velocity magnitudes for the two ends of the raft (a) and the corresponding phase angles (b).

Figure 2 shows the minimum (blue solid line) and maximum (red dash line) cost function obtained searching the sum of the squared velocity magnitudes for the two ends of the raft (a) and the corresponding phase angles (b). The blue circles show the phase that minimizes the cost function and the red squares show the phase which maximizes the cost function. As shown in Fig. 2(a), the first two resonances in the corresponding modes of the system can be clearly recognized. While the third to fifth natural frequencies being too close to each other, the figure cannot show them distinctly. Also, it shows considerable reduction across the frequency range from 0Hz up to 200Hz, especially at the fundamental and sixth natural frequencies. In Fig. 2(b), it is clear that the phase angle either to minimize the cost function or to maximize it between the reference source and the control source is either 0 ºor 180 ºrespectively at almost all of the frequencies evaluated.

Besides, comparing Figures 2(a) and (b), they show that the phase angle to minimize or maximize the cost function shifts from 0 ºto 180 ºor vice versa at two particular frequencies which are around 14.8Hz and 32.4Hz respectively. Moreover, the difference between the minimum and maximum of the cost function at these two frequencies is quite small, which means that around these particular frequencies changing the phase of the two machines would not make much difference to the value of the cost function. This is mainly because that at these two frequencies, the translational and rotational motions of the raft are equally dominant and, since the two sources are positioned at each end of the raft, changing the phase angle of the secondary source may reduce the vertical displacement of the raft but increase the rotation of the raft or vice versa.

3.2 The effect of source isolation

For the model used in this paper, each source mass with its corresponding support isolation can be seen as an uncoupled two degree of freedom mass-spring-damping system. As each single system contains two natural uncoupled frequencies, i.e. the modes being pure vertical motion and pure rotation in the symmetric model case, assume that the corresponding uncoupled natural frequencies of the three subsystems are f_1, f_2 for the machines as well as f_b for the raft, and the rocking frequencies are f_1^R, f_2^R and f_b^R respectively. Clearly, the vertical and rocking natural frequencies of each uncoupled system can be calculated by the equations as follows.

$$f_i = \frac{1}{2\pi}\sqrt{\frac{k_l + k_r}{m_i}} \qquad f_i^R = \frac{1}{2\pi}\sqrt{\frac{(k_l + k_r)(\frac{l_i}{2})^2)}{J_i}}$$

where *i*=1, 2 and *b* indicates the three uncoupled systems and *l*, *r* denotes the corresponding isolations at each end of the three masses.

To compare with the case described in former section, two cases in which the stiffnesses of the isolations for the sources were set to be relatively soft and hard respectively; therefore, the vertical natural frequencies and rotational natural frequencies of each mass for two different cases can be calculated and given in Table 2 below.

Table 2. Natural frequencies of the uncoupled two degree of freedom system for two different cases.

	f_1/Hz	f_2/Hz	f_b/Hz	f_1^R/Hz	f_2^R/Hz	f_b^R/Hz
Case A	90.64	85.07	20.83	155.94	172.15	35.82
Case B	5.23	5.01	20.83	9.00	10.13	35.82

For Case A, the stiffness of the isolations for Machine A were set as $3\times10^{5}\mathrm{Nm}^{-1}$ and that for Machine B was $2.6\times10^{5}\mathrm{Nm}^{-1}$, then the source machine vertical and rotational natural frequencies are greater than that of the raft; while in the Case B, the corresponding stiffnesses were set to $1\times10^{3}\mathrm{Nm}^{-1}$ and $9\times10^{2}\mathrm{Nm}^{-1}$ respectively; so the machine natural frequencies are lower than that of the raft.

Using the same full searching approached at step size of 7.2 ºused in the last section, Figures 3 and 4 show respectively the minimum (blue solid line) and maximum (red dash line) cost function (a) and the corresponding phase angles (b) for Case A and Case B. The blue circles show the phase that minimizes the cost function and the red squares show the phase which maximizes the cost function. From these two figures, similar with what was shown in Figure 2, the phase angles in the two cases between the two machines to achieve minimum or maximum cost function are also 0 º or 180 º respectively. Besides, in Figure 3, there are also two particular frequencies, about 51Hz and 77Hz, for which the phase would shift from 0 º to 180 º or vice versa. In Figure 4, however, the most noteworthy part is that the phase angles to minimize or maximize the cost function did not change to opposition at any frequency. Although, at around 35Hz the cost function did not show any changes with altering the phase angle of the secondary source. The reason is unlike the other two cases, each mode shows quite clear motion of each mass at every natural frequency when the isolators for the sources are soft enough. Therefore, with the changes in the frequency, there will not be the change of the dominant motion of the system. In other words, in this situation, the translational motion of the raft can be seen as the 'dominant movement' in the frequency band of 0Hz to 200Hz as the phase angle that can minimize the cost function remains at 180 º.

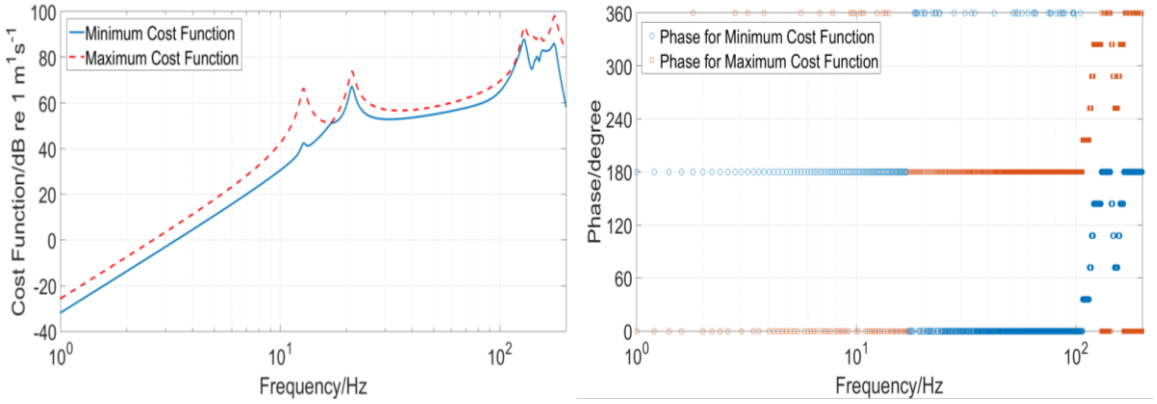

(a) (b)

Figure 3. Plots of the minimum (blue solid line) and maximum (red dash line) cost function (a) and the corresponding phase angles (b) when the stiffnesses of the isolations for the sources are relatively higher than that for the raft.

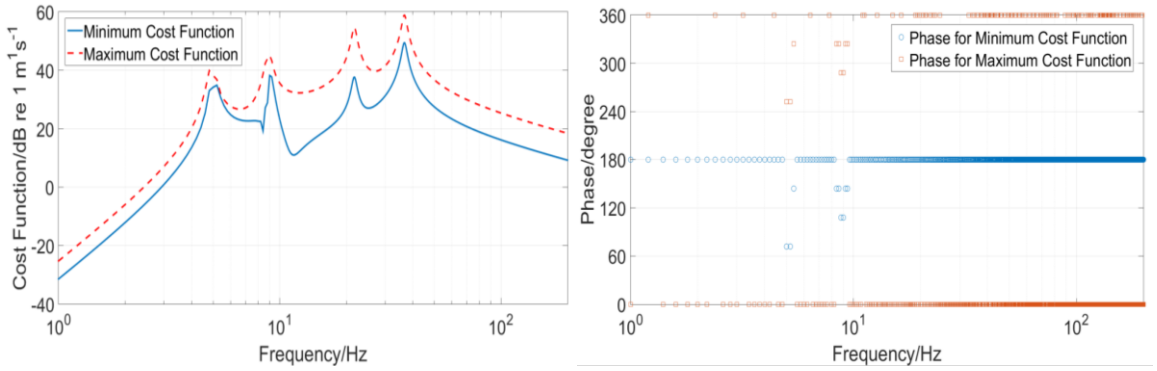

(a) (b)

Figure 4. Plots of the minimum (blue solid line) and maximum (red dash line) cost function (a) and the corresponding phase angles (b) when the stiffnesses of the isolations for the sources are relatively softer than that for the raft.

4. EXPERIMENTAL VALIDATION

4.1 Test rig

A photograph of the experimental test rig is shown in Figure 5(a). A 1.2m×0.102m ×0.025m aluminium box section beam was used as the support platform which was resiliently attached to the ground. On the top the raft, two aluminium smaller plates was mounted by 4 rubber mounts respectively. Each plate supports a Data Physics IV40 inertial shaker. The shakers were installed away from the centre of each plate, in which case, both forces and moments can be introduced into the support raft below. All other relevant properties were used in the numerical simulation described in the previous section. A block diagram of the experimental test rig, including the instrumentation, is shown in Figure 5. One of the shakers (left-hand side one) was to simulate the reference machine, while the other one was used as a control machine, for which the phase was adjustable.

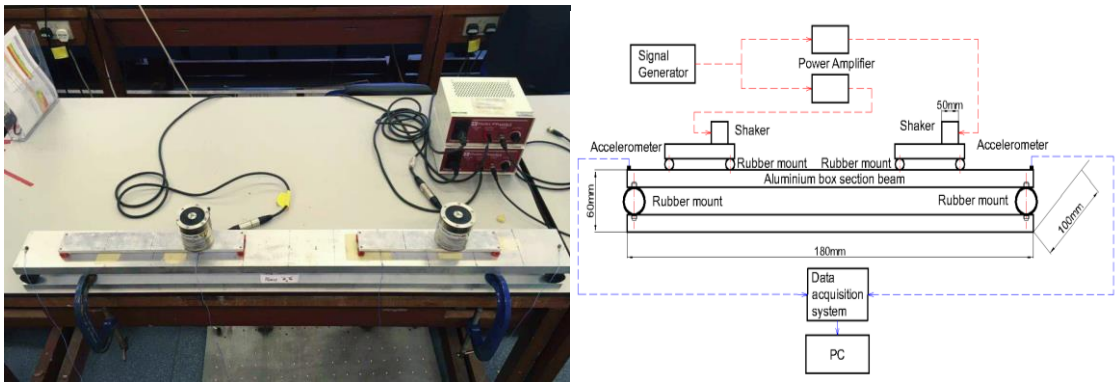

(a) (b)

Figure 5. Photograph of the experimental test rig, details of which can be found in Table 3 (a) and the block diagram of the experimental test rig (b).

4.2 Manual synchrophasing test

As shown in Figure 5(b), the excitation signals supplied to each shaker through the power amplifier were generated by a two-channel signal generator by which the precise phase angle between the two signals can be adjusted manually. Although the phase between the forces applied to the system by the shakers was unknown, measuring the transfer mobilities can take this into account and then be used to determine the optimum phase angle between the driving signals that will minimize or maximize the cost function. Rather than driving the shakers with band limited white noise and measuring the responses of the identical positions, which is not suitable for the real rotating machines as described above, the PST method was used to determine the generalized transfer mobilities at several separate frequencies.

Once the mobilities have been determined, the minimum and maximum cost function as well as the corresponding phase angle can be calculated mathematically and numerically using Matlab. The results of the cost function are shown in Table 4 below.

Table 4. Maximum and minimum value of the cost function calculated by an exhaustive search through 0 ºto 360 ºat certain frequencies using the transfer mobilities determined by the PST.

Frequency/HZ	12	17.5	20	22	24	25	26	28	30	32
Minimum cost function/dB	-37.50	-35.90	-37.50	-35.90	-32.37	-32.37	-24.47	-27.75	-27.41	-20.20
Maximum cost function/dB	-33.12	-29.28	-33.12	-29.28	-28.34	-28.34	-20.85	-17.92	-22.01	-15.51
Frequency/HZ	34	35	36	40	43	50	57	61	80	100
Minimum cost function/dB	-22.75	-24.47	-15.69	-27.75	-22.62	-20.20	-22.75	-15.69	-22.91	-20.40
Maximum cost function/dB	-17.45	-20.85	-11.79	-17.92	-7.16	-15.51	-17.45	-11.79	-12.98	-14.57

It is clear that different levels of reductions of the cost function, from 4dB to 15dB can be achieved using synchrophasing at these particular frequencies. More importantly, the phase angles show how well they agree with the simulation results, especially at the low frequencies. When the excitation frequency was less than 20 Hz, the phase needed to minimize the cost function is 0 ºor 180 ºand the change appears around 16Hz, which is quite similar to the numerical results. On the other hand, however, in the frequency range from 30Hz to 70Hz, although there is a clear shift of the phase angle in the simulation, the experimental results show a more complicated change required for the phase angle due to the elasticity of the raft.

5. CONCLUSION

This paper has extended previous work on synchrophasing vibration control. The experimental validation took place on an aluminium extruded box section beam excited by several shakers, while the shakers in this study were supported by a separated beam and then resiliently attached by four rubber mounts to the host raft. This kind of machinery installation is quite common in reality such as on a ship; therefore, the forces and moments introduced by the machines were taken into account.

As shown both theoretically and experimentally in this paper, adjusting the relative phase angle between the shakers can reduce the cost function which is the sum of the squares of velocities of each end of the raft.

ACKNOWLEDGEMENTS

The authors gratefully acknowledge the financial support from the National Natural Science Foundation of China (No. 51375103).

REFERENCE

1. Yang T.J., Zhang X.Y., Xiao Y.H., et al. Adaptive vibration isolation system for marine engine. Journal of Marine Science and Application, 3, (2), (2004) 30-35.
2. Fuller C.R., Elliott S.J and Nelson P.A., Active Control of Vibration, Academic Press Ltd., 1997.
3. Fuller C.R., Analytical model for investigation of interior noise characteristics in aircraft with multiple propellers including synchrophasing, Journal of Sound and Vibration, 109, (1), (1986) 141-156.
4. Mallock A., A method of preventing vibration in certain classes of steamships, Transactions of the Institute of Naval Architects, 47 (1905) 227-230.

5. Jones J.D., Fuller C.R., Noise-control characteristics of synchrophasing. 1 Experimental Investigation, AIAA Journal, 24 (8) (1986) 1271-1276.
6. Efimtsov B.M., Zverev A.Y., Sound field produced in a shell by 2 synchrophased sources. Soviet Physics Acoustics-USSR, 38, (4), (1992) 382-386.
7. Harada I., Blower noise reducing method by phase control. Patent: JP54060656, 1977.
8. Howard C., Experimental results of synchrophasing two axial fans in a duct. Proceedings of the Active 04 Conference; 20-22 September 2004; Williamsburg, Virginia, USA 2004. Paper No. A04_29.
9. Pla F.G., Goodman G.C., Method and apparatus for synchronizing rotating machinery to reduce noise. United States Patent 5221185, 1993.
10. Pla FG. Method for reducing noise and/or vibration from multiple rotating machines. United States Patent 5789678, 1998.
11. Blunt D.M., Rebbechi B., Propeller synchrophase angle optimisation study. Proceedings of the 13th AIAA/CEA Aeroacoustics Conference; 21-23 May 2007; Rome, Italy, 2007. Paper No. AIAA-2007-3584.
12. Magliozzi B., Adaptive synchrophaser for reducing aircraft cabin noise and vibration. United States Patent 5453943, 1995.
13. Johnston J.F., Donham R.E., Guinn W.A., Propeller signatures and their use. AIAA Journal of Aircraft, 18, (11), (1981) 934-942.
14. Dench M.R., Brennan M.J., Ferguson N.S., On the control of vibrations using synchrophasing. Journal of Sound and Vibration. 332 (2013) 4842-4855.
15. Yang T.J., Zhou L.B, Brennan M.J., et al., On synchrophasing control of vibration for a floating raft vibration isolation system. INTER-NOISE and NOISE-CON Congress and Conference Proceedings. Vol. 249, No. 3 (2014), Institute of Noise Control Engineering.